Composite Structures 215 (2019) 289–297

Contents lists available at ScienceDirect

Composite Structures

journal homepage: www.elsevier.com/locate/compstruct

3D topology optimization of continuous fiber-reinforced structures via natural evolution method

Alexander A. Safonov

Center for Design, Manufacturing and Materials, Skolkovo Institute of Science and Technology, Moscow, Russia

ARTICLE INFO

Keywords:
Topology optimization
SIMP
Composite additive manufacturing
3D printing
Orientation design

ABSTRACT

The method to optimize a topology of 3D continuous fiber-reinforced additively manufactured structures is discussed. The proposed method makes it possible to simultaneously search for density distribution and local reinforcement layup in 3D composite structures of transversely isotropic materials. The approach uses a dynamical systems method to find density distribution, combined with the method for rotation of reinforcement direction to align it in the direction of principal stresses with local minimum compliance. The algorithm is implemented as a built-in material model within Abaqus finite element suite. Both the optimal material density distribution and the distribution of fiber orientation vector are determined for three structural elements used as benchmarks: the bending of simply supported 2D beam under central point load, the loading of 3D cube by vertical load, and the bending of 3D cantilever beam.

1. Introduction

The last years have seen the rapid development in the application of 3D printing technologies for fabrication of various fiber-reinforced plastic structures [1]. A good example is a fabrication of continuous fiber-reinforced thermoplastic structures by modified fused-deposition modeling (FDM) process [2]. Thermoplastic filament and continuous fiber are separately fed into a 3D printer (see Fig. 1a). Inside a heated nozzle of a printing head a filament is heated to a melting point and a hot melt thermoplastic impregnates a reinforcing fiber immediately before printing [3]. Continuous fiber-reinforced (CFR) printed composites can outperform regular 3D printed polymer composites by an order of magnitude [4]. Custom built software plugin translates the digital model of a structure into a set of commands for a 3D printer, defining the layout of reinforced and non-reinforced plastic, and specifying the orientation of reinforcement. Fig. 1b shows a sample CFR 3D printed part fabricated by the Anisoprint process [5]. Robotic systems can further improve 3D printing capabilities (see Fig. 1c), allowing a fabrication of large composite parts with complex spatial architecture and higher content of reinforcing fibers [1]. However, optimized design methods should be used to make the most of these capabilities. Thus, one of the primary goals is a development of structural optimization methods for composite structures, allowing high mechanical performance to be achieved with minimum weight of structure. This implies a capability to simultaneously search for density distribution and local orientation of reinforcement in 3D composite structures.

An extensive research in the field of spatial optimization of structures is currently under way [6,7]. Standard method of topology optimization consists in modeling the layout of material using the parameter of material density, ρ, varying from 0 to 1, which corresponds respectively to the absence or presence of material, and where the relation between structural properties and the density of material is described by a power law. This method is known as Solid Isotropic Material with Penalization (SIMP) [6,8]. Thus, the optimization of objective function is reduced to finding an optimum distribution of ρ: $\min f(\rho)$. However, with models of over 1000 elements, common in engineering practice, the application of non-gradient methods for topology optimization become prohibitively expensive [9]. Among several available gradient-based topology optimization methods [10–12] of special note is the method stemming from the fact that topology optimization problem can be reduced to a problem of finding a stationary point of an Ordinary Differential Equation (ODE) [13]. Considering density constraints, ρ, the right term of ODE is equal to a projected negative gradient of the objective function. Numerical schemes of topology optimization solution can be found using simple explicit Euler algorithm. As shown in [14], iterative schemes match the algorithms used in bone remodeling literature [15]. A connection between optimization algorithms and natural phenomena such as amoeboid organism growing toward food sources [16,17], and formation of natural sandstone arches [18,19] is also shown.

The most obvious approach to simultaneous optimization of material distribution and orientation for 2D composite structures consists in

E-mail address: a.safonov@skoltech.ru.

https://doi.org/10.1016/j.compstruct.2019.02.063
Received 7 February 2018; Received in revised form 30 December 2018; Accepted 15 February 2019
Available online 19 February 2019

Fig. 1. Fabrication of 3D continuous fiber reinforced printed parts by Anisoprint process [5]: (a) – process scheme, (b) – the sample of optimized CFR 3D printed frame of a quadrocopter, (c) – 6-axis robotic cell prototype (ProM-PT).

application of classical topology optimization tools to find material distribution while orienting reinforcing fibers along the principal stress direction (fiber steering technique) [20]. This approach is based on the fact that in case of a plane problem with orthotropic material extreme energy values are achieved when principal directions for material, stresses and strains coincide [21,22]. Although in extreme cases there may exist optimal solutions with coinciding directions of principal stresses and strains not aligned in the direction of material principal axes. In [22,23] authors concluded that for shear weak materials the optimum fiber orientation coincides with the principal stress direction. Besides, for the 3D case, as was found in [24,25], principal directions of stresses and strains are coincident for critical values of strain energy density. For the transversely isotropic material a constraint for the elastic constants has been established, such that the global energy minimum can only be reached when axis of anisotropy is aligned with one of the principal stress axes [25]. As shown in [26], the results obtained with the principal stress method [27] are very close to those obtained using the general stress based optimality criteria method [28]. Setoodeh [29] proposed a method of simultaneous fiber path and topology design of composite laminae using a cellular automata (CA) framework. General topology optimization method with continuous and discrete orientation design using isoparametric projection was discussed in [30,31]. Although the number of works on combined design for orientation and topology is small [29,32], several interesting problems for 2D composite structures have been successfully solved, such as the plate with a centrally located circular hole [33,34], cantilever plates [29,31,34], membrane structures [35], compliant mechanisms [32].

All studies discussed above deal with optimization of reinforcement lay-up in 2D objects, such as plates or membranes. However, in order to optimize 3D printed composite structures 3D topology optimization methods tailored for continuous fiber-reinforced structures should be developed. This article discusses a method of simultaneous search for density distribution and a fiber orientation vector in 3D composite structures of transversely isotropic materials. The approach proposed here uses a dynamical systems method to find density distribution [13,14], combined with the method of orienting the reinforcement in the direction of principal stress with minimum compliance [27]. Optimum material density distribution and distribution of fiber orientation vector are determined for three structural elements used as benchmarks: 2D beam, 3D cube, and 3D cantilever beam. Results are compared with those obtained by Setoodeh in [29] for 2D cantilever beams.

2. Method

A classical problem of topology optimization consists in finding the optimum layout of material within a structure to ensure its maximum stiffness [6]. In other words, the problem is to find an optimum distribution of material density ρ and a local reinforcement (fiber orientation) vector $\mathbf{n}$ within a given volume Ω, such that compliance is minimal [36]:

$$\text{Minimize } C(\rho, \boldsymbol{n}) = \frac{1}{2}\int_{\Omega} \{\varepsilon_{xyz}\}^T \cdot E^*(\rho, \boldsymbol{n}) \cdot \{\varepsilon_{xyz}\} d\Omega, \tag{1}$$

where

$$E^*(\rho, \boldsymbol{n}) = \rho^p E(\boldsymbol{n}), \quad p > 1. \tag{2}$$

The following constraints are imposed on density, ρ, distribution:

$$\int_{\Omega} \rho d\Omega \le M; \quad 0 < \rho_{\min} \le \rho \le 1. \tag{3}$$

The notation used in equations above is as follows: $\{\varepsilon_{xyz}\}$ – strains in Voigt notation, $E^*(\rho, \boldsymbol{n})$ – transformed local stiffness matrix in xyz-coordinates, $E(\boldsymbol{n})$ – transformed local stiffness matrix at $\rho(x) = 1$, M – constraint on total amount of material, p – penalization power ($p > 1$), ρ_{min} – minimum density. It is assumed that composite material is transversely isotropic and the axis of anisotropy is directed along the local vector of reinforcement $\boldsymbol{n}$. Let us write $E(\boldsymbol{n})$ using the stiffness matrix of transversely isotropic material in the principal coordinate system (123-coordinates) $[Q]$, which is the inverse of the compliance matrix $[S]$ [37],

$$[\mathrm{E}(\mathbf{n})] = [\mathrm{T}] \bullet [\mathrm{Q}] \bullet [\mathrm{R}] \bullet [\mathrm{T}]^{-1} \bullet [\mathrm{R}]^{-1} \tag{4}$$

where $[\mathrm{Q}] = [\boldsymbol{S}]^{-1}$, and [S] is the compliance matrix in principal coordinate system,

$$[\mathrm{S}] = \begin{bmatrix} 1/E_1 & -\nu_{12}/E_1 & -\nu_{12}/E_1 & 0 & 0 & 0 \\ -\nu_{12}/E_1 & 1/E_2 & -\nu_{23}/E_2 & 0 & 0 & 0 \\ -\nu_{12}/E_1 & -\nu_{23}/E_2 & 1/E_2 & 0 & 0 & 0 \\ 0 & 0 & 0 & 1/G_{23} & 0 & 0 \\ 0 & 0 & 0 & 0 & 1/G_{12} & 0 \\ 0 & 0 & 0 & 0 & 0 & 1/G_{12} \end{bmatrix} \tag{5}$$

[R] is Reuter's matrix,

$$[\mathrm{R}] = \begin{bmatrix} 1 & 0 & 0 & 0 & 0 & 0 \\ 0 & 1 & 0 & 0 & 0 & 0 \\ 0 & 0 & 1 & 0 & 0 & 0 \\ 0 & 0 & 0 & 2 & 0 & 0 \\ 0 & 0 & 0 & 0 & 2 & 0 \\ 0 & 0 & 0 & 0 & 0 & 2 \end{bmatrix} \tag{6}$$

[T] is the transformation matrix [38],

$$[\mathrm{T}] = \begin{bmatrix} a_{11}^2 & a_{12}^2 & a_{13}^2 & 2a_{12}a_{13} & 2a_{13}a_{11} & 2a_{11}a_{12} \\ a_{21}^2 & a_{22}^2 & a_{23}^2 & 2a_{22}a_{23} & 2a_{23}a_{21} & 2a_{21}a_{22} \\ a_{31}^2 & a_{32}^2 & a_{33}^2 & 2a_{32}a_{33} & 2a_{33}a_{31} & 2a_{31}a_{32} \\ a_{21}a_{31} & a_{22}a_{32} & a_{23}a_{33} & a_{22}a_{33}+a_{23}a_{32} & a_{21}a_{33}+a_{23}a_{31} & a_{22}a_{31}+a_{21}a_{32} \\ a_{31}a_{11} & a_{32}a_{12} & a_{33}a_{13} & a_{12}a_{33}+a_{13}a_{32} & a_{13}a_{31}+a_{11}a_{33} & a_{11}a_{32}+a_{12}a_{31} \\ a_{11}a_{21} & a_{12}a_{22} & a_{13}a_{23} & a_{12}a_{23}+a_{13}a_{22} & a_{13}a_{21}+a_{11}a_{23} & a_{11}a_{22}+a_{12}a_{21} \end{bmatrix} \tag{7}$$

(a_{11}, a_{21}, a_{31}) coincides with the components of vector $\mathbf{n}$, (a_{12}, a_{22}, a_{32}) and (a_{13}, a_{23}, a_{33}) coincide with vectors appending to orthonormal basis.

Following are the iterative algorithms used to find density ρ and a local vector of reinforcement $\mathbf{n}$.

2.1. Density

In accordance with the SIMP method the region being studied can be divided in finite elements with varying material density values assigned to each finite element [6]. Here, the material density ρ_i is determined for each integration point of each finite element. In order to solve the problem (1)–(7) we apply the approach used in dynamical systems modeling [13].

Let us assume that ρ depends on a time-like variable t, and consider the following differential equation to determine density in i-th integration point ρ_i when solving the problem stated in (1)–(3):

$$\dot{\rho}_i = \lambda\left(\frac{pC_i(\rho_i, n_i)}{\rho_i} - \mu V_i\right), \quad C_i(\rho_i, n_i) = \frac{1}{2}\int_{\Omega_i}\{\varepsilon_{xyz}\}^T E^*(\rho, n)\{\varepsilon_{xyz}\}d\Omega, \tag{8}$$

where dot above denotes the derivative with respect to t; Ω_i is a domain of i-th integration point; V_i is a volume of a domain of i - th integration point; λ is a physical dimensional positive constant; μ is a positive parameter that regulates the relative importance of the cost function (1) and of the mass constraint (3). We can obtain this equation by applying methods of projected dynamical systems [39], or bone remodeling method [15,40,41]. Klarbring [8,9] has given the detailed description of relations between Optimality Criteria (OC) method [6], method of dynamical system, and bone remodeling method. It should be noted that the term $\frac{pC_i(\rho_i, \mathbf{n_i})}{\rho_i}$ is the negative derivative of the compliance. The parameter μ is selected during the calculations so as to satisfy the mass constraint (3). A standard method of finding μ is using the bi-sectioning algorithm [36]. In all calculations presented below the value of μ at each iteration step is determined accurate to 10^{-4}.

For numerical solution of Eq. (5) we use a projected Euler method [43], giving an iterative formulation for a solution to ρ_i [23]:

$$\rho_i^{n+1} = \rho_i^n + q\left[\frac{pC_i(\rho_i^n, n_i^n)}{\rho_i^n V_i} - \mu^n\right] \tag{9}$$

where $q = \lambda\Delta t$, $\rho_i^{n+1}$and ρ_i^n – numerical approximations of $\rho_i(t + \Delta t)$ and $\rho_i(t)$.

To avoid the necessity of using the trial and error method to find the dimensional parameter q in Eq. (9), when solving practical problems of structures optimization we consider a modified algorithm based on dimensionless parameters. As multiplication of the right term of Eq. (8) by a positive function does not affect the result of optimization [13], following modification can be considered:

$$\rho_i^{n+1} = \rho_i^n + \Delta\rho_i^n, \tag{10}$$

where $\rho_i^0 = \rho_0$ – specified initial value of density, and $\Delta\rho_i^n$ – is taken as follows

$$\Delta\rho_i^n = \begin{cases} K\Delta\rho_i^{n-1} if\left(\frac{pC_i(\rho_i^n, \mathbf{n}_i^n)}{\rho_i^n V_i} - \mu^n\right)\Delta\rho_i^{n-1} > 0, \\ -\Delta\rho_i^{n-1}/K if\left(\frac{pC_i(\rho_i^n, \mathbf{n}_i^n)}{\rho_i^n V_i} - \mu^n\right)\Delta\rho_i^{n-1} \le 0, \end{cases} \tag{11}$$

where $\Delta\rho_i^0 = k_0$; K, k_0 – positive constants. With matching signs of equation $\left(\frac{pC_i(\rho_i^n, \mathbf{n}_i^n)}{\rho_i^n V_i} - \mu^n\right)$ and previous increment $\Delta\rho_i^{n-1}$ the current increment $\Delta\rho_i^n$ increases in $K \ge 1$ times compared to $\Delta\rho_i^{n-1}$, therefore the K parameter is introduced to accelerate algorithm convergence rate. Otherwise, the increment $\Delta\rho_i^n$ will decrease K times and reverse its sign.

After a value of ρ_i^{n+1} is calculated using Eq. (12), we make a projection onto a set of constraints for ρ_i:

$$\rho_i^{n+1} = \begin{cases} 1 & if\rho_i^{n+1} > 1 \\ \rho_i^{n+1} & if\rho_{min} \le \rho_i^{n+1} \le 1 \\ \rho_{min} & if\rho_{min} > \rho_i^{n+1} \end{cases} \tag{12}$$

Discretization approach considered here can result in numerical instabilities such as mesh dependence and checkerboard patterns [42]. In order to overcome possible problems, author applies the density filtering method [36], meaning that density ρ_i within all modeling domain is replaced by filtered density value when calculating mechanical characteristics (2). The filtering consists in smoothing the density value over adjacent integration points and is implemented as follows [13]:

$$\bar{\rho}_j = \sum_{i=1}^{E}\Psi_{ji}\rho_i, \quad j = 1, \cdots, E. \tag{13}$$

Here

$$\Psi_{ij} = \frac{\psi_{ij}V_j}{\sum_{k=1}^{E}\psi_{ik}V_k}, \quad \psi_{ij} = \max\left(0, 1 - \frac{|\boldsymbol{e_i} - \boldsymbol{e_j}|}{R}\right), \tag{14}$$

where $\mathbf{e_i}$ denotes the position vector of the integration point i and R is the filter radius, V_j – volume of j-th integration point.

2.2. Local vector of reinforcement

In [25] the constraint for the elastic constants of transversely isotropic material is obtained, such that global energy minimum is reached only when the axis of anisotropy is aligned with one of the principal stress axes. The constraint consists in negative value of the parameter $a = S_{11} + S_{33} - 2S_{13} - 4S_{55}$, where S_{11}, S_{33}, S_{13}, S_{55} – elements of the compliance matrix [S] (5). For the transversely isotropic material used further (see Table 1) this condition is satisfied: $a = -0.517\ \mathrm{GPa}^{-1} < 0$. The algorithms considered here are a development of these ideas in a form of evolutionary algorithm, aimed to minimize the compliance of 3D structures. The iterative formulation used to find reinforcement direction is expressed as a rotation of a current position of reinforcement axis $\mathbf{n}_i^n$ in i-th integration point toward the selected direction of principal stress, in the following form:

$$\mathbf{n}_i^{n+1} = \mathbf{M}(\nu_i^n, \omega)\bullet\mathbf{n}_i^n, \tag{15}$$

where $\mathbf{M}(\nu_i^n, \omega)$ – the matrix of rotation by the angle of ω about the axis given by the unit vector $\nu_i^n = (\alpha, \beta, \gamma)$; $\nu_i^n = \mathbf{n}_i^n \times \mathbf{n}_{\boldsymbol{p}_i}^n$ – vector product of the vector of current position of reinforcement axis $\mathbf{n}_i^n$ and the vector of chosen principal direction of stresses $\mathbf{n}_{\boldsymbol{p}_i}^n$. The rotation matrix $\mathbf{M}(\nu_i^n, \omega)$ is determined as follows

Table 1
Algorithm parameters used in simulation.

p	R	K	k_0	ρ_{min}	ω
3	1.42	1.2	0.01	0.01	5°

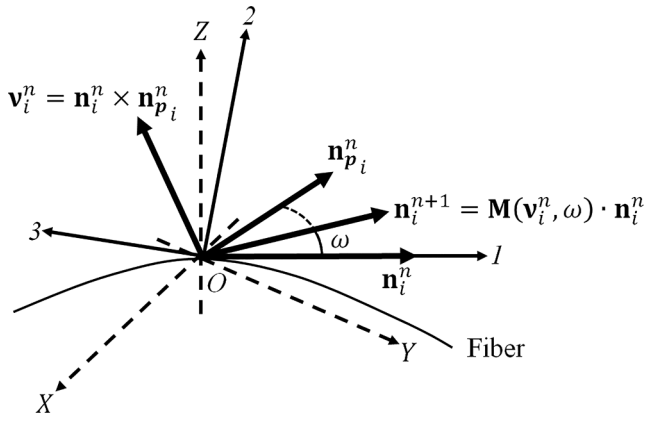

Fig. 2. Illustration of the algorithm used to find the optimum direction of reinforcement, where O123 – principal coordinate system of a material; and OXYZ – natural coordinate system; $\mathbf{M}(\nu_i^n, \omega)$ – the matrix of rotation by the angle of ω about the axis given by the unit vector ν_i^n; $\nu_i^n = \mathbf{n}_i^n \times \mathbf{n}_{p_i}^n$ – vector product of the vector of current position of reinforcement axis $\mathbf{n}_i^n$ and the vector of chosen principal direction of stresses $\mathbf{n}_{p_i}^n$.

$$\mathbf{M}(\nu_i^n, \omega) = \begin{pmatrix} \cos\omega + (1 - \cos\omega)\alpha^2 & (1 - \cos\omega)\alpha\beta - (\sin\omega)\gamma & (1 - \cos\omega)\alpha\gamma + (\sin\omega)\beta \\ (1 - \cos\omega)\beta\alpha + (\sin\omega)\gamma & \cos\omega + (1 - \cos\omega)\beta^2 & (1 - \cos\omega)\beta\gamma - (\sin\omega)\alpha \\ (1 - \cos\omega)\gamma\alpha - (\sin\omega)\beta & (1 - \cos\omega)\gamma\beta + (\sin\omega)\alpha & \cos\omega + (1 - \cos\omega)\gamma^2 \end{pmatrix} \tag{16}$$

Fig. 2 illustrates the iterative algorithm used to find the optimum direction of reinforcement.

Let us consider the evolutionary heuristic method to find the vector of chosen principal direction of stress, $\mathbf{n}_{p_i}^n$. The method consists in rotating the current position of reinforcement axis $\mathbf{n}_i^n$ to align it with the principal stress vector $\mathbf{n}_{\alpha i}^n$ with minimum local compliance for the stresses $\{\sigma_{xyz}\}$. The principal direction is chosen using the following expression:

$$\mathbf{n}_{p_i}^n = \text{argmin}_{\mathbf{n}_{\alpha i}^n}\left(\frac{1}{2}\{\sigma_{xyz}\}^T \bullet [\mathrm{E}^*(\rho_i^n, \mathbf{n}_{\alpha_i}^n)]^{-1} \bullet \{\sigma_{xyz}\}\right), \quad \alpha = 1, 2, 3, \tag{17}$$

where $\mathbf{n}_{\alpha i}^n$ – the principal stress vector; $\mathrm{E}^*(\rho_i^n, \mathbf{n}_{\alpha_i}^n)$ – the transformed stiffness matrix where a local vector of reinforcement coincides with $\mathbf{n}_{\alpha i}^n$; $\{\sigma_{xyz}\}$ – the stresses. The expression (17) includes the principal stress vector $\mathbf{n}_{\alpha i}^n$ such that the local compliance for local stresses $\{\sigma_{xyz}\}$ for transformed stiffness matrix $\mathrm{E}^*(\rho_i^n, \mathbf{n}_{\alpha_i}^n)$ is minimal.

The number of independent design variables used to find the density (12)–(16) and the direction of reinforcement (17) can be estimated by multiplying the number of elements in a model, the number of integration points in the element of a given type, and the number of design variables for each integration point (the density and 2 independent design variables for the direction of reinforcement in the 3D setting). For example, for a 3D model of 10 000 8-node linear brick elements the number of independent design variables will constitute 240 000.

2.3. Implementation within Abaqus environment

The algorithm shown above is implemented within Abaqus environment with user subroutines Uexternaldb, Urdfil, Usdfld [43]. We use Uexternaldb subroutine to set specific parameters of the algorithm, Urdfil — to access the results of solution of stress-strain distribution by Abaqus Solver, and Usdfld procedure — to account for changes in mechanical properties. In order to parameterize the local vector of reinforcement $\mathbf{n}_i^n$ using Usdfld procedure the spherical coordinate system is used

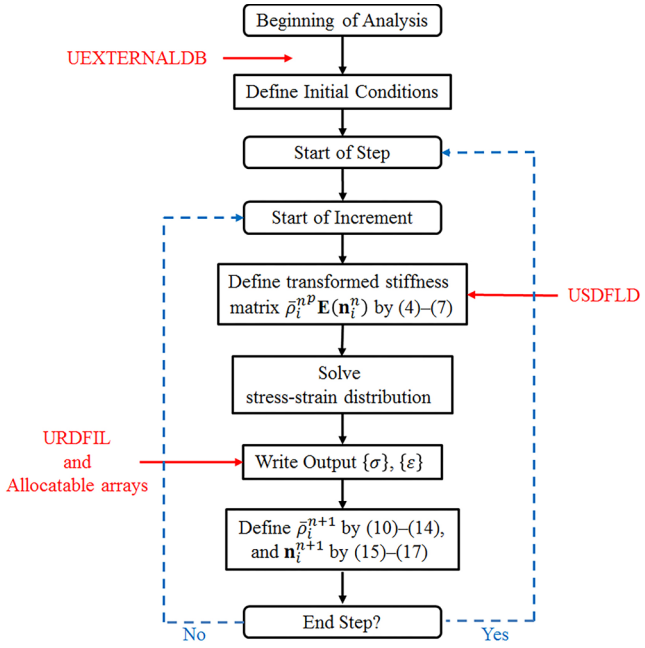

Fig. 3. The flowchart of optimization process implementation within Abaqus environment.

$$\mathbf{n}_i^n = (\cos\theta, \sin\theta\cos\varphi, \sin\theta\sin\varphi), \tag{18}$$

where θ – polar angle ($0Â° \le \theta \le 90Â°$) and φ – azimuthal angle ($-180Â° \le \varphi \le 180Â°$). The uniform grid with $10Â°$ increments was used to partition values of θ and φ angles.

Fig. 3 shows the flowchart of optimization process implementation within ABAQUS environment. Subroutines hook-up locations are marked with red. When solving sample problems and comparing results to those stated in Setoodeh's work [29], the search for optimal solution is stopped when relative difference in compliance values obtained in any two pairs of last 5 iterations does not exceed 10^{-4}.

We would like to note that the developed plug-in allows optimization of computational models built with different types of finite elements with different number of integration points, taking into account contact interactions and geometric nonlinearity. In addition to the possibility of optimizing the density distribution or the reinforcement orientation separately, the plug-in also allows users to isolate certain parts of computational model, not to be optimized. Moreover, users can set different values of filter radii for density distribution and reinforcement direction optimization, allowing for variations in typical dimensions of structural elements and for reinforcement orientation variability.

Although a uniform rectangular mesh of the same finite elements was used in the sample problems, the proposed method and developed plug-in allow optimization of an arbitrary mesh of finite elements. The method was called NEAM (Natural Evolution Anisotropic Material) as it is based on the evolutionary behavior of mechanical or biological systems, and is implemented as a material model.

3. Results and discussion

3.1. Comparison with the previous research data

In this section we present results obtained with proposed method, compared with those obtained by Setoodeh in [29]. We used data on mechanical properties presented in [29]. The values of the algorithm parameters are given in the Table 1. Two predictive models are

Table 2
Normalized compliance values for cantilever plates from Setoodeh et al.[29], and obtained using the proposed method.

Volume fraction (target mean density ρ_{ev}^{∞})	Normalized compliance	
	Proposed Method (19)	Setoodeh [29]
Symmetric cantilever plate (325 × 82 finite elements)		
0.3	1.86	2.22
0.5	1.12	1.14
Asymmetric cantilever plate (203 × 102 finite elements)		
0.5	0.53	0.47

considered: symmetric cantilever plate with aspect ratio of 4:1 (325x82 finite elements) and asymmetric cantilever plate with aspect ratio of 2:1 (203x102 finite elements). Table 2 shows the values of normalized compliance with respect to a 0° fiber design with initial mean density $\rho_{ev}^{0} = 10.0$ for reviewed models with various target values of mean density $\rho_{ev}^{\infty} = M/V$ (volume fraction) for the proposed method, and the results from [29]. The initial position of the axis of anisotropy coincides with OX axis for all elements.

For the symmetric cantilever plate we were able to obtain better optimized solutions using the proposed method. Moreover, for the volume fraction of $\rho_{ev}^{\infty} = 0.3$ the compliance of the structure obtained with proposed method was 20% less compared to that obtained by Setoodeh [29]. However, in case of the asymmetric cantilever plate the proposed method results in a less stiffer structure compared to that obtained by Setoodeh [29], with 11% higher compliance. Unfortunately, Setoodeh [29] did not specify the method used to apply load, which is essential for the problems being solved. This is especially true for the case of asymmetric cantilever plate, where a substantial vertical load is applied to the corner area, creating the considerable stress concentration zone. Also, Setoodeh [29] did not specify absolute compliance values for initial 0° fiber design with initial mean density $\rho_{ev}^{0} = 10.0$, and for obtained optimized structures. Due to this fact, it is not possible to validate the models described here against models used by Setoodeh [29]. It is also necessary to note that other research works on the subject of simultaneous optimization of density / reinforcement orientation mentioned in Introduction section lack the data necessary to conduct a full scale comparison of reported optimization results with structures obtained with algorithm proposed here.

3.2. Sample problems

Here we present the detailed description of computations conducted for sample 2D and 3D structures. To test the developed algorithm three sample problems were used: the bending of simply supported 2D beam under central point load; the loading of 3D cube by vertical central load; the bending of 3D cantilever beam (see Fig. 4).

The first problem deals with optimization of a flat rectangular beam under a point load $F = -200$ kN acting in downward direction and applied to the center of the upper side of the beam. A half of the model is considered (see Fig. 4). That is why we apply the vertical load of $F/2$ to the upper left corner of the model, uniformly distributed between 2 nodes of the finite element adjacent to the upper left corner of the model. Zero vertical movement conditions are imposed on the lower right vertex. The length of the model is $a = 150$ m, and the height of the model is $b = 50$ m. Design domain is modeled by a mesh of $150 \times 50 \times 1$ cubic C3D8-type elements with 8 integration points. Final compliance value for target mean density ρ_{ev}^{∞} was set equal to 0.3. The number of design variables used in finding density distribution alone constitutes 60 000. For a simultaneous search of density distribution and reinforcement direction the number of design variables involved will constitute 180 000.

The second problem is the optimization of a 3D cube under the vertical point load $F = -900$ kN applied to the center of the upper face and uniformly distributed between 9 nodes of 4 finite elements adjacent to the center of the of the upper face and located on the upper face (see Fig. 4). The model is rigidly fixed at its lower face vertices, and constraints are imposed on the square pads with dimensions of 2×2 m, adjacent to the vertices. The length of the cube edge is $c = 20$ m. Design domain is modeled by a mesh of $20 \times 20 \times 20$ of C3D8-type cubic elements with 8 integration points. Final compliance value for target mean density ρ_{ev}^{∞} was set equal to 0.1. The number of design variables used in finding density distribution constitutes 64 000. For a simultaneous search of density distribution and reinforcement direction this number will constitute 192 000.

The third problem is the optimization of a 3D cantilever beam under the vertical point load $F = -200$ kN acting in downward direction and applied to the center of the extreme lower horizontal face. A half of the model is considered. Zero displacement conditions are imposed on the opposite vertical faces. The length of the model is $d = 40$ m, the height is $e = 20$ m and the width of the model is $f = 10$ m. Design domain is modeled by a mesh of $40 \times 20 \times 10$ cubic C3D8-type elements with 8 integration points. Final compliance value for target mean density ρ_{ev}^{∞} was set equal to 0.1. The number of design variables used to find density distribution alone constitutes 64 000. For a simultaneous search of density distribution and reinforcement direction the number of design variables involved will constitute 192 000.

Table 3 lists mechanical properties of materials used in calculations: the unidirectionally reinforced (UD) material, the quasi-isotropic laminate (QIL), the 3D quasi-isotropic bulk (QIB) material. The quasi-isotropic laminate (QIL) is built with UD material [37]. 3D QIB material is an artificial isotropic material built with UD material. Properties of UD and QIL materials are taken from [37]. Properties of QIB material are proposed by the author of this work. Table 1 lists algorithm parameters used in solution of sample problems considered here. The angle of rotation ω is reduced linearly to the value of $\omega/10$ during the first 225 iterations, and then remains constant.

Table 4 shows simulation results for sample problems and material types discussed earlier. Fig. 5 shows distributions of density and reinforcement orientation angle for sample problems discussed earlier for UD material; proposed method (18) is used to determine position of the axis of anisotropy in each element, the initial position of the axis

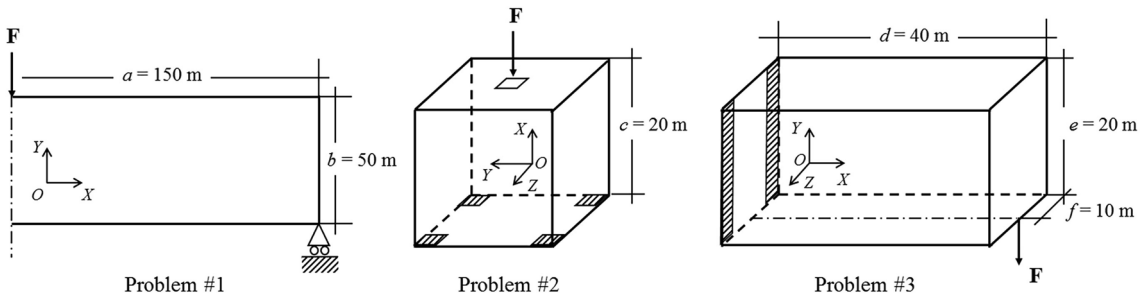

Fig. 4. Sample problems: Problem #1 – bending of a 2D beam under central point load (MBB-beam problem); Problem #2 – loading of a 3D cube by vertical load; Problem #3 – loading of a 3D cantilever beam by vertical load.

Table 3
Mechanical properties of materials used in simulation.

Properties	Unidirectional reinforced material (UD) [37]	Quasi-isotropic laminate (QIL) [37]	Quasi-isotropic bulk (QIB)
E_1 (GPa)	100.00	38.99	25.00
E_2 (GPa)	10.00	11.79	25.00
G_{12} (GPa)	3.00	3.21	9.40
ν_{12}	0.30	0.33	0.33
ν_{23}	0.45	0.30	0.33

coincides with *OX* axis.

Of special interest is a comparison of final values of compliance for UD material obtained by simultaneous optimization of density / reinforcement orientation with initial and final values of compliance for materials when density distribution is optimized separately (see Table 4). Thus, compliance values obtained for final structures with $\rho_{ev}^{\infty} = 0.3$ *(2D beam) and* $\rho_{ev}^{\infty} = 0.1$ *(3D cube, 3D cantilever beam)* are close to initial compliance values for structures with $\rho_{ev}^{0} = 1.0$. Besides, the final compliance value for structures where density distribution is optimized separately is 3 times higher compared to "fiber steered" structures. As virtual composite materials considered here are composed of the same source material by changing its lay-up, it can be concluded that optimization of local reinforcement orientation allows a significantly stiffer structures to be obtained, compared to structures with uniform lay-up of reinforcement.

3.3. Influence of algorithm parameters and modifications

Algorithm parameters used in sample problems were selected during solution of 2D beam problems. Number of iterations in all calculations presented later was set at 300. Final density distribution $\bar{\rho}_i$ for QIB material was obtained with different filter radii $R \in \{0.00, 0.60, 0.80, 1.00, 1.20, 1.42, 1.75, 2.00, 2.25, 2.42\}$. Final values of mean density and compliance for analyzed filter radii R are given in Table 5. For $R \in \{0.00, 0.60, 0.08, 1.00\}$ checkerboard-patterned regions can be observed in some areas. The size of checkerboard regions decreases with increase in filter radius. For other analyzed filter radii no checkerboard regions were observed. The increase in filter radius results in a less detailed structure and, consequently, in increased compliance. In order to prevent formation of checkerboard regions and excessively detailed structures the radius of $R = 1.42$ was chosen for analysis.

Table 6 shows simulation results for QIB material with varying parameters k_0 and K defining convergence rate of the algorithm (11). Various combinations of $k_0 \in \{0.002,\ 0.010\}$ and $K \in \{1.0,\ 1.2,\ 1.4\}$ parameters were studied. Other parameters remained constant (see Table 1). To evaluate the rate of convergence in compliance calculations a parameter $N_{1\%}$ is introduced, equal to the number of the iteration starting from which the relative difference between current C^n and final C^{300} values of compliance would not exceed 1%, i.e., $\forall\ n > N_{1\%}$: $\frac{|C^n - C^{300}|}{C^{300}} 100\% < 1\%$. For $K = 1.0$ the density increment at each iteration step remains constant and equal $\Delta\rho_i^n = k_0$. In this case ($K = 1.0$) with $k_0 = 0.002$ the algorithm fails to converge to a stable structure within 300 iterations. At $k_0 = 0.01$ the algorithm is able to converge to a stable structure, with $N_{1\%} = 170$. When algorithm acceleration is used a significant reduction in $N_{1\%}$ can be observed, up to the $N_{1\%} = 117$, i.e. the number of iterations required to find optimum solution is reduced while retaining the final stiffness value of the obtained solution $C^{300} = 60.4$ J.

Table 7 shows final values of compliance for different values of rotation angle, $\omega \in \{2.5°, 5.0°, 10.0°, 20.0°\}$. Position of the axis of anisotropy in each element is determined by proposed method (17). The lowest compliance value was obtained for $\omega = 5°$, that is why it was selected for calculations (see Table 1).

3.4. Algorithm modifications

We also considered following modifications of proposed method: the use of Optimality Criteria method [36] to find density distribution, and the use of the method of direct alignment of reinforcement in the direction of principal stresses with minimal compliance to find optimum reinforcement orientation

$$\mathbf{n}_i^{n+1} = \mathrm{argmin}_{\mathbf{n}_{\alpha i}^n} (\{\sigma_{xyz}\}^T \bullet [\rho_i^n,\ \mathrm{E}^*(\mathbf{n}_{\alpha i}^n)]^{-1} \bullet \{\sigma_{xyz}\}), \qquad \alpha = 1,\ 2,\ 3. \tag{19}$$

Table 8 shows final values of compliance for different combinations of considered methods used in the 2D beam problem for the UD material. Parameters for Optimality Criteria method were taken from [36].

Table 4
Simulation results for the sample problems.

Type of simulation	Initial compliance for initial mean density $\rho_{ev}^{0} = 1.0$, J	Final compliance for target mean density ρ_{ev}^{∞}, J
2D beam ($\rho_{ev}^{\infty} = 0.3$)		
QIB material	23.3	60.0
QIL material, plane of isotropy coincides with OXY plane	16.3	44.1
UD material, position of the axis of anisotropy for all finite elements is constant and coincides with OX axis	16.6	50.8
UD material, proposed method (18) is used to determine position of the axis of anisotropy in each element, initial position of the axis coincides with OX axis	16.6	20.0
3D cube ($\rho_{ev}^{\infty} = 0.1$)		
QIB material	7.2	31.9
QIL material, plane of isotropy coincides with *OXY* plane	7.3	40.7
UD material, position of the axis of anisotropy for all finite elements is constant and coincides with *OX* axis	7.5	54.5
UD material, proposed method (18) is used to determine position of the axis of anisotropy in each element, initial position of the axis coincides with *OX* axis	7.5	9.3
3D cantilever beam ($\rho_{ev}^{\infty} = 0.1$)		
QIB material	14.9	27.1
QIL material, plane of isotropy coincides with *OXY* plane	15.3	26.7
UD material, position of the axis of anisotropy for all finite elements is constant and coincides with *OX* axis	18.5	31.8
UD material, proposed method (18) is used to determine position of the axis of anisotropy in each element, initial position of the axis coincides with *OX* axis	18.5	10.5

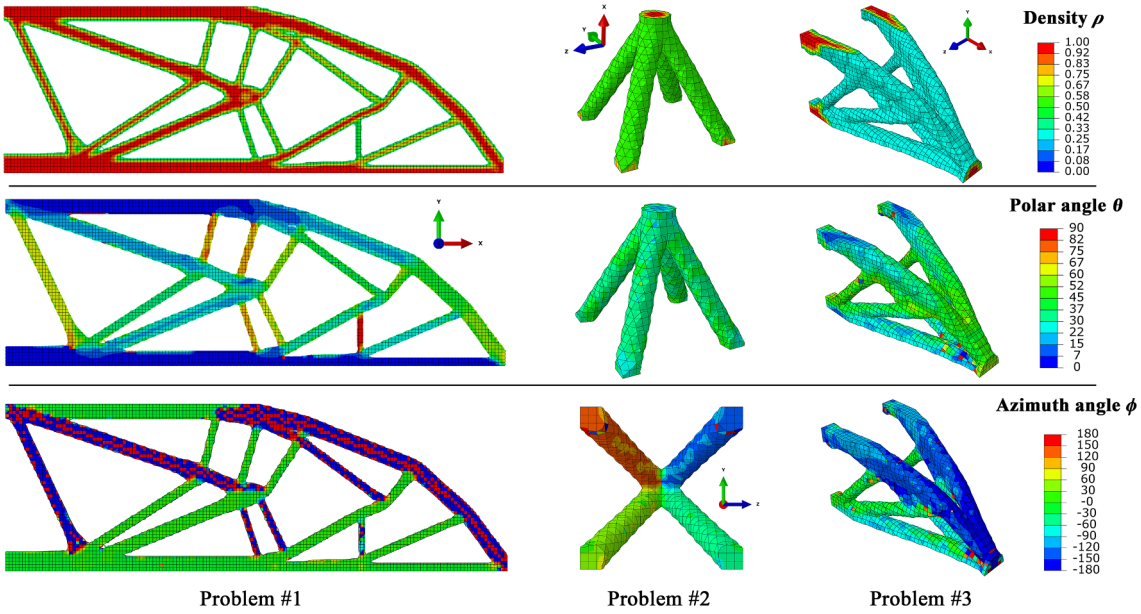

Fig. 5. The final distribution of density $\bar{\rho}$, polar angle θ, and azimuth angle φ for sample problems discussed earlier in case of UD material; proposed method (18) is used to determine position of the axis of anisotropy in each element, initial position of the axis coincides with OX axis. Where ($0Â° \le \theta \le 90Â°$) – the polar angle between OX axis and direction of reinforcement, ($-180Â° \le \varphi \le 180Â°$) – the azimuth angle between OY axis and projection of direction of reinforcement onto OYZ plane. Regions with densities exceeding 0.3 are shown, i.e. $\bar{\rho} > 0.3$.

Table 5
Final values of compliance for QIB material, obtained with different filter radii R.

	Filter radius R									
	0.00	0.60	0.80	1.00	1.20	1.42	1.75	2.00	2.25	2.42
Compliance C^{300}, J	62.5	65.6	68.4	62.5	58.7	60.0	62.8	63.3	65.8	65.5

Table 6
Simulation results for varying k_0 and K parameters determining convergence rate of the algorithm (11) for QIB material.

k_0	K	C^{300}, J	$N_{1\%}$
0.002	1.0	100.2	None
	1.2	61.0	213
	1.4	62.3	118
0.010	1.0	60.4	170
	1.2	60.4	117
	1.4	60.8	185

Table 7
Final values of compliance for UD material, obtained for various rotation angle values ω after 300 iterations.

	Rotation angle, ω			
	2.5°	5.0°	10.0°	20.0°
Compliance C^{300}, J	22.4	21.2	24.0	22.6

The lowest compliance value was obtained for the method proposed here.

We afford speculations that the density search algorithm (10)–(14) may be considered as a continual generalization of evolutionary algorithms such as ESO [44] and BESO [45]. It is obvious, that by assigning unit values to algorithm parameters K and k_0, and by varying the total amount of material M one can obtain the evolutionary algorithm for compliance calculation, similar to methods mentioned earlier. Moreover, the density search algorithm (10)–(14) can be modified by substituting the compliance with other physical quantities, e.g. with various stress tensor invariants. Thus, the use of the trace of a stress tensor was considered in [18] to describe the erosion process. The algorithm described here can also be used to find the optimum distribution of heat conductive material in the heat conduction problem [46]. Proposed modifications of the algorithm will be discussed in future works.

In this paper we propose the method to determine the optimal distribution of material and direction of reinforcement within a given domain. These data can be used as inputs for 3D composite printer instructions describing the regions with reinforced and non-reinforced plastic, and the orientation of reinforcement by specifying layup direction. At the same time, the paper does not cover shell elements, common in traditional composite structures analysis and allowing engineer to specify the multiple ply layups with interlaced orientations. However, the method proposed here can be applied with such elements as computations are done at integration points and the number of points can be specified for each separate ply. Future research will focus at improvement of the algorithm to account for differences in elastic modulus in tension and compression, local buckling of structural elements, and advanced strength criteria for thermoplastic materials [47]. We also intends to further refine the algorithms, considering manufacturing constraints imposed by conventional processes of composite structures fabrication, such as autoclave forming [48], vacuum infusion [49], winding [50], and pultrusion [51].

4. Conclusion

A method of topology optimization for three-dimensional continuous fiber-reinforced structures fabricated by composite additive manufacturing process has been developed. The method is based on a dynamic approach to finding the optimum configuration for local distribution of material density. Iterative algorithms for material density have been developed, with algorithm parameters being dimensionless quantities. In order to find the reinforcement vector evolutionary algorithm is proposed based on method for rotation of reinforcement direction to align it in the direction of principal stresses. The algorithms

Table 8
Final values of compliance obtained for 2D beam problem for UD material, for different combinations of proposed method, the Optimality Criteria method, and method of direct alignment of reinforcement in the direction of principal stresses.

	Proposed method (10–17)	Optimality Criteria method to find density distribution + evolutionary method to find reinforcement orientation (17)	Evolutionary method to find density distribution (10)–(14) + method of direct alignment of reinforcement orientation (19)	Optimality Criteria method to find density distribution + of direct alignment method to find reinforcement orientation (19)
Compliance, J	20.00	22.3	20.7	20.9

are implemented as a plug-in within ABAQUS environment, via user subroutines Usdfld, Urdfil, Uexternaldb. Applicability of the method is demonstrated by solving a problem of finding optimal distributions for material density and reinforcement vector for transversely isotropic material with properties typical of continuous fiber-reinforced composites for the cases of bending of simply supported 2D beam under central point load, loading of 3D cube by vertical load, and bending of the 3D cantilever beam. It was found that proposed algorithm produces lighter structures (by 66% and 90% in case of 2D beam and 3D cube/beam, respectively) with stiffness virtually equivalent to that of initial structures of anisotropic and quasi-isotropic materials. The results obtained can also be used as a benchmark for future studies. Dimensionless parameters of the algorithm were found, ensuring its good convergence and allowing optimization of 3D printed continuous fiber reinforced structures under service loads to be performed in engineering practice.

Acknowledgements

Author would like to express his sincere gratitude to Professor Stepan Lomov for his support and help in proofreading the article. Author would also like to thank Dr. Boris Fedulov for his valuable comments on the algorithm of density calculation, and Dr. Anton Trofimov for his comments on the algorithm of finding the direction of reinforcement. Author is grateful to Dr. Fedor Antonov, CEO of Anisoprint LLC, for consulting on design and operation of 3D continuous fiber reinforced composite printer. This research did not receive any specific grant from funding agencies in the public, commercial, or not-for-profit sectors.

References

[1] Zhang Y, De Backer W, Harik R, Bernard A. Build orientation determination for multi-material deposition additive manufacturing with continuous fibers. Procedia CIRP 2016;50:414–9. https://doi.org/10.1016/j.procir.2016.04.119.
[2] Parandoush P, Lin D. A review on additive manufacturing of polymer-fiber composites. Compos Struct 2017;182:36–53. https://doi.org/10.1016/J.COMPSTRUCT.2017.08.088.
[3] Matsuzaki R, Ueda M, Namiki M, Jeong T-K, Asahara H, Horiguchi K, et al. Three-dimensional printing of continuous-fiber composites by in-nozzle impregnation. Sci Rep 2016;6:23058. https://doi.org/10.1038/srep23058.
[4] Melenka GW, Cheung BKO, Schofield JS, Dawson MR, Carey JP. Evaluation and prediction of the tensile properties of continuous fiber-reinforced 3D printed structures. Compos Struct 2016;153:866–75. https://doi.org/10.1016/j.compstruct.2016.07.018.
[5] Azarov AV, Antonov FK, Vasil'ev VV, Golubev MV, Krasovskii DS, Razin AF, et al. Development of a two-matrix composite material fabricated by 3D printing. Polym Sci – Ser D 2017:10. https://doi.org/10.1134/S1995421217010026.
[6] Bendsoe MSO. Topology optimization: theory, methods, and applications. Springer Science & Business Media; 2003.
[7] Aage N, Andreassen E, Lazarov BS, Sigmund O. Giga-voxel computational morphogenesis for structural design. Nature 2017:550. https://doi.org/10.1038/nature23911.
[8] Bendsøe MP. Optimal shape design as a material distribution problem. Struct Optim 1989;1:193–202. https://doi.org/10.1007/BF01650949.
[9] Rozvany GIN. A critical review of established methods of structural topology optimization. Struct Multidiscip Optim 2009;37:217–37. https://doi.org/10.1007/s00158-007-0217-0.
[10] Sigmund O, Maute K. Topology optimization approaches: a comparative review. Struct Multidiscip Optim 2013;48:1031–55. https://doi.org/10.1007/s00158-013-0978-6.
[11] Svanberg K. The method of moving asymptotes – a new method for structural optimization. Int J Numer Methods Eng 1987;24:359–73. https://doi.org/10.1002/nme.1620240207.
[12] Ostanin I, Tsybulin I, Litsarev M, Oseledets I, Zorin D. Scalable topology optimization with the kernel-independent fast multipole method. Eng Anal Bound Elem 2017:83. https://doi.org/10.1016/j.enganabound.2017.07.020.
[13] Klarbring A, Torstenfelt B. Dynamical systems and topology optimization. Struct Multidiscip Optim 2010;42:179–92. https://doi.org/10.1007/s00158-010-0479-9.
[14] Klarbring A, Torstenfelt B. Dynamical systems, SIMP, bone remodeling and time dependent loads. Struct Multidiscip Optim 2012:45. https://doi.org/10.1007/s00158-011-0724-x.
[15] Harrigan TP, Hamilton JJ. Bone remodeling and structural optimization. J Biomech 1994:27. https://doi.org/10.1016/0021-9290(94)90008-6.
[16] Safonov A, Jones J. Physarum computing and topology optimisation. Int J Parallel Emergent Distrib Syst 2017;32:448–65. https://doi.org/10.1080/17445760.2016.

1221073.
[17] Jones J, Safonov A. Slime mould inspired models for path planning: collective and structural approaches. In: Adamatzky A, editor. Shortest Path Solvers. From Softw. to Wetware Cham: Springer International Publishing; 2018. p. 293–327. https://doi.org/10.1007/978-3-319-77510-4_11.
[18] Ostanin I, Safonov A, Oseledets I. Natural erosion of sandstone as shape optimisation. Sci Rep 2017;7:17301. https://doi.org/10.1038/s41598-017-17777-1.
[19] Safonov AA. Computing via natural erosion of sandstone. Int J Parallel Emergent Distrib Syst 2018:1–10. https://doi.org/10.1080/17445760.2018.1455836.
[20] Ghiasi H, Fayazbakhsh K, Pasini D, Lessard L. Optimum stacking sequence design of composite materials part II: variable stiffness design. Compos Struct 2010;93:1–13. https://doi.org/10.1016/j.compstruct.2010.06.001.
[21] On Pedersen P. optimal orientation of orthotropic materials. Struct Optim 1989:1. https://doi.org/10.1007/BF01637666.
[22] Pedersen P. Bounds on elastic energy in solids of orthotropic materials. Struct Optim 1990. https://doi.org/10.1007/BF01743521.
[23] Banichuk NV. Optimization of anisotropic properties of deformable media in plane problems of elasticity. Mech Solids 1979;14:63–8.
[24] Rovati M, Taliercio A. Stationarity of the strain energy density for some classes of anisotropic solids. Int J Solids Struct 2003. https://doi.org/10.1016/S0020-7683(03)00371-8.
[25] Norris AN. Optimal orientation of anisotropic solids. Q J Mech Appl Math 2006. https://doi.org/10.1093/qjmam/hbi030.
[26] Cheng HC, Kikuchi N, Ma ZD. An improved approach for determining the optimal orientation of orthotropic material. Struct Optim 1994. https://doi.org/10.1007/BF01743305.
[27] Suzuki K, Kikuchi N. A homogenization method for shape and topology optimization. Comput Methods Appl Mech Eng 1991. https://doi.org/10.1016/0045-7825(91)90245-2.
[28] Hassani B, Hinton E. Review of homogenization and topology optimization III – topology optimization using optimality criteria. Comput Struct 1998. https://doi.org/10.1016/S0045-7949(98)00133-3.
[29] Setoodeh S, Abdalla MM, Gürdal Z. Combined topology and fiber path design of composite layers using cellular automata. Struct Multidiscip Optim 2005. https://doi.org/10.1007/s00158-005-0528-y.
[30] Nomura T, Dede EM, Lee J, Yamasaki S, Matsumori T, Kawamoto A, et al. General topology optimization method with continuous and discrete orientation design using isoparametric projection. Int J Numer Methods Eng 2015;101.. https://doi.org/10.1002/nme.4799.
[31] Lee J, Kim D, Nomura T, Dede EM, Yoo J. Topology optimization for continuous and discrete orientation design of functionally graded fiber-reinforced composite structures. Compos Struct 2018;201:217–33. https://doi.org/10.1016/j.compstruct.2018.06.020.
[32] Tong X, Ge W, Zhang Y. Optimal fiber orientation and topology design for compliant mechanisms with fiber-reinforced composites. Proc Inst Mech Eng Part C J Mech Eng Sci 2017;231:2302–12. https://doi.org/10.1177/0954406216631783.
[33] Hyer MW, Charette RF. Use of curvilinear fiber format in composite structure design. AIAA J 1991:29. https://doi.org/10.2514/3.10697.
[34] Pedersen P. On thickness and orientational design with orthotropic materials. Struct Optim 1991:3. https://doi.org/10.1007/BF01743275.
[35] Klarbring A, Torstenfelt B, Hansbo P, Larson MG. Optimal design of fibre reinforced membrane structures. Struct Multidiscip Optim 2017;56.. https://doi.org/10.1007/s00158-017-1685-5.
[36] Sigmund O. A 99 line topology optimization code written in matlab. Struct Multidiscip Optim 2001:21. https://doi.org/10.1007/s001580050176.
[37] Akkerman R. On the properties of quasi-isotropic laminates. Compos Part B Eng 2002;33:133–40. https://doi.org/10.1016/S1359-8368(02)00002-1.
[38] Newnham RE. Properties of Materials: Anisotropy, Symmetry, Structure. Oxford: Oxford University Press; 2005.
[39] Nagurney AZD. Projected Dynamical Systems and Variational Inequalities with Applications. New York: Springer Science & Business Media; 1996.
[40] Huiskes R, Rulmerman R, Van Lenthe GH, Janssen JD. Effects of mechanical forces on maintenance and adaptation of form in trabecular bone. Nature 2000:405. https://doi.org/10.1038/35015116.
[41] Payten WM, Ben-Nissan B, Mercer DJ. Optimal topology design using a global self-organisational approach. Int J Solids Struct 1998;35.
[42] Sigmund O, Petersson J. Numerical instabilities in topology optimization: a survey on procedures dealing with checkerboards, mesh-dependencies and local minima. Struct Optim 1998;16:68–75. https://doi.org/10.1007/BF01214002.
[43] Abaqus Analysis User Manual, Version 6.14. (2014). n.d. http://www.3ds.com/productsservices/.
[44] Xie YM, Steven GP. A simple evolutionary procedure for structural optimization. Comput Struct 1993:49. https://doi.org/10.1016/0045-7949(93)90035-C.
[45] Querin OM, Steven GP, Xie YM. Evolutionary structural optimisation (ESO) using a bidirectional algorithm. Eng Comput (Swansea, Wales) 1998:15. https://doi.org/10.1108/02644409810244129.
[46] Safonov A, Adamatzky A. Computing via material topology optimisation. Appl Math Comput 2018;318:109–20. https://doi.org/10.1016/j.amc.2017.08.030.
[47] Fedulov BN, Safonov AA, Kantor MM, Lomov SV. Modelling of thermoplastic polymer failure in fiber reinforced composites. Compos Struct 2017;163:293–301. https://doi.org/10.1016/j.compstruct.2016.11.091.
[48] Peeters DMJ, Hesse S, Abdalla MM. Stacking sequence optimisation of variable stiffness laminates with manufacturing constraints. Compos Struct 2015. https://doi.org/10.1016/j.compstruct.2015.02.044.
[49] Barnes RH, Morozov EV. Structural optimisation of composite wind turbine blade structures with variations of internal geometry configuration. Compos Struct 2016. https://doi.org/10.1016/j.compstruct.2016.05.013.
[50] Vasiliev VV, Barynin VA, Razin AF. Anisogrid composite lattice structures – development and aerospace applications. Compos Struct 2012;94.. https://doi.org/10.1016/j.compstruct.2011.10.023.
[51] Safonov AA, Carlone P, Akhatov I. Mathematical simulation of pultrusion processes: a review. Compos Struct 2018:184. https://doi.org/10.1016/j.compstruct.2017.09.093.